RELATING PERFORMANCE AND STRUCTURE OF NANOCOMPOSITES BY NEW METHODS IN TIME-RESOLVED X-RAY SCATTERING

N. Stribeck*, A. Zeinolebadi, M. Ganjaee Sari
Dept. of Chemistry, University of Hamburg, 20146 Hamburg, Germany
* Norbert Stribeck(norbert@stribeck.de)

Keywords: *Nanocomposites, CNT, SAXS, mechanical loading*

Abstract. Small-angle X-ray scattering (SAXS) has been used to monitor slow mechanical tests of polypropylene and a nanocomposite containing multi-wall carbon-nanotubes. By comparing the extracted evolution information on nanostructure to the mechanical data it has been found that the moderate improvement of mechanical properties (change from necking to homogeneous straining) appears to be related to an increased extension of crystalline lamellae and to an inhibition of nanostructure fatigue in the composite. In the oral presentation we will compare these results to nanocomposites in which CNT is replaced by layered silicates. In this case the crystallites in the nanocomposites are not bigger, but many small crystallites are observed (nucleating effect of layered silicates).

1 Introduction

Polypropylene [1] (PP) is the material preferred [2] by automotive industry for replacement of metal by plastics for reduction of weight and fuel consumption. As it comes to weight reduction of load-bearing components, the materials properties of the polymer are insufficient. A problem solution is the use of hybrid modules from PP and metal that cause high production cost. One could get around the cost if one would succeed to develop an easily processable, low-fatigue PP-based composite. Glass-fiber reinforced PP-composites [3,4] are well introduced and exhibit advanced properties. Nevertheless, the production of the molded parts is still elaborate, because at least the rupture of the glass fibers must be minimized. Thus, carbon nanotubes or graphenes bonded with PP could become an economical alternative.

In service, materials are frequently subjected to strain or cyclic loading. Hence, resistance [5] to dynamic load (i.e. low fatigue [6–8]) is required. There is abundant experimental literature on the relation between materials structure and mechanical load [9]. Nevertheless, the number of papers in which scattering is studied simultaneously during fatigue tests is still small [10,11]. Fortunately, recent progress at synchrotron x-ray radiation facilities makes it possible to follow the variation of anisotropic scattering patterns of polymers during mechanical tests with sufficient accuracy.

2 Experimental

Materials.

Isotactic polypropylene (PP) and a composite (PP+CNT) from 99.9 wt.-% PP and 0.1 wt.-% multi-wall carbon nanotubes (CNT) have been studied.

Components.

Isotactic polypropylene (PP) from Lyondell-Basell has been used. The grade is Moplen HP 400R (density 0.90 g/cm ^{3} , melt flow rate 25 g/ 10 min, melting temperature 161 $^\circ$ C). The commercial CNT-grade is obtained from MK Nano, Canada (MWCNT, +95% Pure, OD: 10-20 nm, -OH functionalized, -OH content 3.06 et%, specific surface >200 m ^{2} /g, lot #0420). The length of the nanotubes is 30 µm.

Composite preparation.
The mixture of PP and CNT has been compounded twice into pellets using a Prism Eurolab 16 twin-screw extruder operated at 300 rpm, a temperature of 200 ° C, and a feeding rate providing approximately 1/3 of the max. torque of the extruder. The screws have been set in a strong configuration with 3 mixing zones having 90 ° spaced mixing disks as part of the zone.

Injection molding.
Test bars S3 according to DIN 53504 have been injection molded in a MiniJet II (Thermo Scientific) from a melt of 200 ° C. Mold temperature: 30 ° C, molding pressure: 650 bar, molding time: 45 s. holding pressure: 100 bar. Holding time: 20 s. The cross-section of the parallel central part is ca. 2 mm 1 mm.

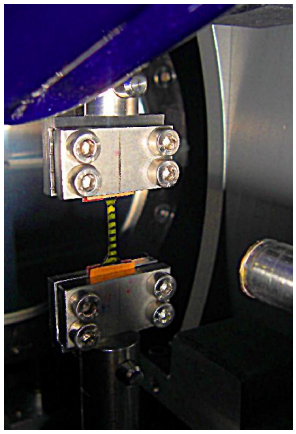

Figure 1: PP+CNT. Setup tensile tester in the synchrotron beamline A2 at HASYLAB, Hamburg

Tensile testing.
Tensile testing is performed in a self-made [12] machine mounted in the synchrotron beam (Fig. 1). A grid of fiducial marks is printed on the test bars [13]. The clamping distance is 30 mm. A 100 N load cell is used. Signals from load cell and transducer are recorded during the experiment. The sample is monitored by a TV-camera. Video frames are grabbed every 10 s and stored together with the experimental data. The machine is operated at a cross-head speed of 0.167 mm/min. Using the fiducial marks the local strain $\varepsilon=(\ell-\ell_0)/\ell_0$ is computed automatically [14] from the average initial distance, ℓ_0, of the fiducial marks and the respective actual distance, ℓ. The true stress, $\sigma=F/A$, is computed from the force F measured by the load cell after subtracting the force exerted by the upper sample clamp, and $A=A_0/(1+\varepsilon)$, the estimated actual sample cross-section. A_0 is the initial cross section of the central zone of the test bar. The equation assumes conservation of sample volume.

In the load-cycling experiments the samples are pre-strained by 1 mm. After that the cycling starts. In each cycle the samples are strained by 0.5 mm and retracted by the same draw-path thereafter.

SAXS setup.
Small-angle X-ray scattering (SAXS) is carried out in the synchrotron beamline A2 at HASYLAB, Hamburg, Germany. The wavelength of radiation is 0.15 nm, and the sample-detector distance is 3031 mm. Scattering patterns are collected by a 2D marccd 165 detector (mar research, Norderstedt, Germany) in binned 1024 1024 pixel mode (pixel size: 158.2 µm 158.2 µm). Scattering patterns are recorded every 30 s with an exposure of 20 s. The scattering patterns are normalized and background corrected [15]. This means intensity normalization for constant primary beam flux, zero absorption, and constant irradiated volume V_0. Because the flat samples are wider than the primary beam, the correction has been carried out assuming $V(t)/V_0=(1/(1+\varepsilon(t)))^{0.5}$. The equation assumes constant sample volume.

SAXS data evaluation.
The scattering patterns $I(s)=I(s_{12},s_3)$ are transformed into a representation of the nanostructure in real space. The only assumption is presence of a multiphase topology. The result is a multidimensional chord distribution function (CDF), $z(r)$ 16. The method is exemplified in

a textbook (Stribeck [15], Sect. 8.5.5). The CDF with fiber symmetry in real space, $z(r_{12},r_3)$, is computed from the fiber-symmetrical SAXS pattern, $I(s_{12},s_3)$, of a multi-phase material. $s=(s_{12},s_3)$ is the scattering vector with its modulus defined by $|s|=s=(2/\lambda)\sin\theta$. λ is the wavelength of radiation, and 2θ is the scattering angle. In order to compute $z(r_{12},r_3)$, $I(s_{12},s_3)$ is projected on the representative fiber plane. Multiplication by s^2 applies the real-space Laplacian. The density fluctuation background is determined by low-pass filtering. It is eliminated by subtraction. The resulting interference function, $G(s_{12},s_3)$, describes the ideal multiphase system. Its 2D Fourier transform is the sought CDF. In the historical context the CDF is an extension of Ruland's interface distribution function (IDF) [17] to the multidimensional case or, in a different view, the Laplacian of Vonk's multidimensional correlation function [18]. The CDF is an "edge-enhanced autocorrelation function" [19–22] – the autocorrelation of the gradient field, $\nabla\rho(r)$. Thus as a function of ghost displacement r, the multidimensional CDF $z(r)$ shows peaks wherever there are *domain surface contacts* between domains in $\rho(r)$ and in its displaced ghost. Such peaks $h_i(r_{12},r_3)$ are called [17] distance distributions. Distance is the ghost displacement. It is sometimes useful to replace the index i by a sequence of indices that indicate the sequence of domains that have been passed along the displacement path until the considered domain surface contact occurs. E.g. $h_{ca}(r_{12},r_3)$ indicates the passing of an amorphous and a crystalline domain.

3 Results and discussion

Tensile tests as a function of CNT content have shown that the mechanical properties are almost constant for CNT contents between 0.05 wt.-% and 3 wt.-%. The stress-strain curves of ordinary tensile tests for the pure PP and the studied nanocomposite are presented in Fig. 2. During straining the pure PP develops a neck, whereas the composite PP+CNT is straining homogeneously. The dynamic driving signal in the load cycling experiments is the cross-head distance. The local macroscopic strain $\varepsilon(t)$ is monitored independently (Fig. 3).

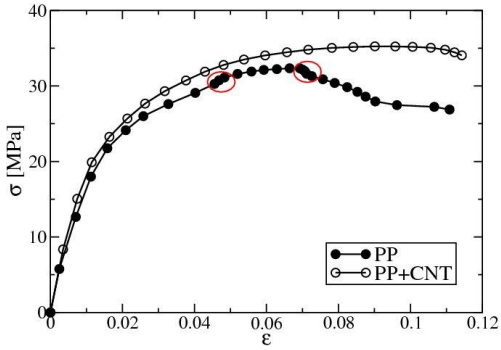

Figure 2: Simple tensile test. PP shows necking. PP+CNT strains homogeneously

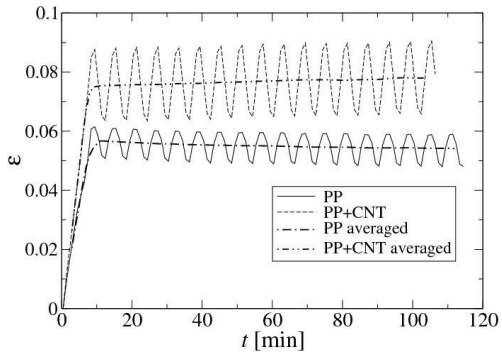

Figure 3: Load cycling (stimulus: technical strain). Local macroscopic strain $\varepsilon(t)$ at the position of X-ray beam irradiation.

$\varepsilon(t)$ of the sample that undergoes necking yields a lowered local strain level and amplitude. Dotted curves are running averages of the oscillating curves. The macroscopic responses of the materials to the driving signal are presented in Fig. 4. Comparison shows that the addition of CNT does not significantly change the fatigue due to stress relaxation. Figure 5 presents selected small-angle scattering patterns recorded in-situ during the load-cycling

experiments.

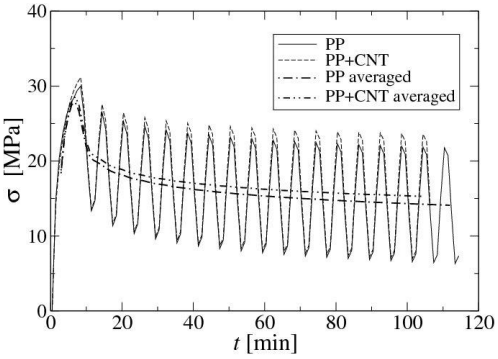

Figure 4: Load cycling of PP and a nanocomposite. Macroscopic mechanical response: true stress $\sigma(t)$

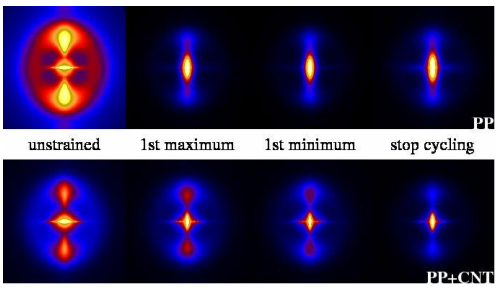

Figure 5: Load cycling. Selected SAXS scattering patterns of pure PP and nanocomposite (PP+CNT)

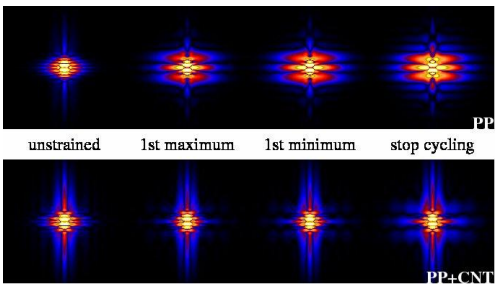

Figure 6: Load cycling. Selected chord distribution functions (CDFs) of pure PP and nanocomposite (PP+CNT) as computed from SAXS

After the 1st maximum has been reached, the changes of the patterns are rather small. Thus the patterns are subjected to the adapted nanostructure analysis method that has been developed by some of us for low-amplitude load-cycling experiments [14,23]. In a first step, a real-space representation (CDF) of the nanostructure is obtained by a modified Fourier analysis. Corresponding patterns are presented in Fig. 6. The CDFs are made from domain-shape distribution-peaks that can be identified and analyzed [14,23] directly without separation, if they are strong. From the strong peak that describes the distance between neighboring crystalline lamellae (long-period peak) several responses of the nanostructure to the dynamic experiment can be extracted. From the variation of the peak position during the dynamic experiment ε_n is obtained. ε_n is the nanoscopic strain in the direction of strain experienced by the semicrystalline stacks (Fig. 7). The curves show that the addition of CNT effectively suppresses the nanostructure fatigue. Moreover, the amplitudes and levels are very similar although these parameters differ considerably in the macroscopic local strains.

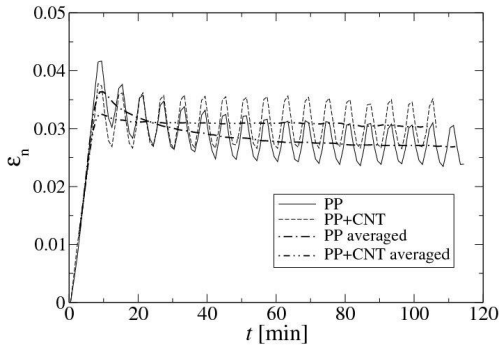

Figure 7: Load cycling of PP and a nanocomposite. Response of nanostructure in straining direction: nanoscopic strain $\varepsilon_n(t)$ from the response of the SAXS long period $L(t)$ extracted from the CDFs

From the shape of the peak in straining direction the heterogeneity of the nanostructure has been extracted. It shows a dynamic oscillation on a low level and is almost identical for both samples. The lateral extension $e_{ca}(t)$ of the crystalline lamellae is extracted from the lateral

breadth of the long-period peak (Fig. 8) We observe that the addition of MWCNT increases "diameter" of the crystalline lamellae considerably. This is the main difference between the nanostructures of PP and PP+CNT,

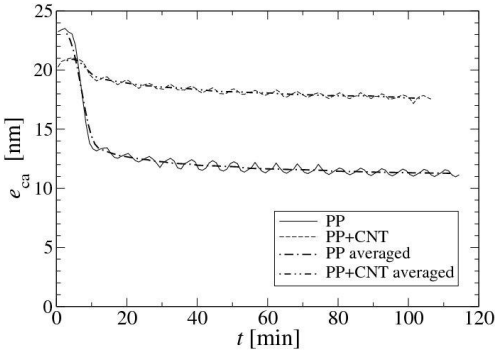

Figure 8: Load cycling of PP and a nanocomposite. Response of nanostructure transverse to the straining direction: extension $e_{ca}(t)$ of the crystallites in the direction perpendicular to strain determined from the breadth of the long period extracted from the CDFs

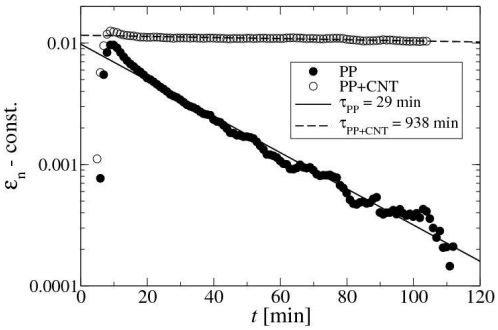

Figure 9: Load cycling of PP and a nanocomposite. Response of nanostructure in the straining direction. Lifetime determination

respectively. The predominant effect is a drop of e_{ca} only for PP during the 1st straining branch. It is related to considerable crumbling of crystalline layers in pure PP, but not in the nanocomposite.

Quantification of fatigue.

In order to quantify the fatigue related to different structural and mechanical responses, the averaged response curves are plotted in a semi-logarithmic plot (cf. Fig. 9) and a constant is subtracted until the curves are linearized. Then the data are fitted to an exponential decay,

$$f(t) = A\exp(-t/\tau),$$

with τ the lifetime of the decay. For the macroscopic stress-relaxation fatigue the analysis yields a life-time of $\tau \approx 45$ min for both materials under the slow cycling conditions. According to Fig. 9 an improvement of the nanoscopic strain-fatigue from PP to the nanocomposite by a factor of 30 is obtained. It must be mentioned that the required linearization introduces some uncertainty that is in the order of 5 min for low lifetimes and 200 min for $\tau \approx 1000$ min. We obtain almost identical values for PP and PP+CNT in the fatigue analyses of the long-period hetero-geneity ($\tau \approx 45$ min) and of the lateral extension of the lamellae ($\tau \approx 60$ min).

4 Conclusions

The results show that subtle changes of mechanical and nanostructural parameters can be recorded with sufficient precision in *in situ* time-resolved SAXS experiments. Fatigue behavior is clearly detected. In order to further study the mechanisms of fatigue from the recorded data, the series of anisotropic scattering data must be analyzed in more depth with respect to nanostructure evolution. The already existing bottleneck of data evaluation will become more severe, when we will be able to increase the strain rates after the start of PETRA III operation at the synchrotron in Hamburg. Nevertheless, with further improved

data analysis tools and instrumentation detailed evolution data of macroscopic mechanical parameters and nanoscopic structural parameters from time-resolved scattering studies will become available. We believe that these results will shed new light upon the relation between mechanical properties and the structure of polymer materials.

Acknowledgments. The authors thank the Hamburg Synchrotron Radiation Laboratory (HASYLAB) for beam time granted in the frame of projects II-2008-0015 and I-2011-0087. This work has been supported by the 7th framework program of the European Union (Project NANOTOUGH FP7-NMP-2007-LARGE).

References

[1] Varga J (1995) Crystallization, melting and supermolecular structure of isotactic polypropylene, in *Polypropylene: Structure, blends and composites* (Ed. Karger-Kocsis J), Chapman & Hall, London, chap. 3, pp. 51–106.

[2] Edwards K L (2004) Strategic substitution of new materials for old: Applications in automotive product development, *Mater Des* **25**:529–533.

[3] Youssef Y and Denault J (1998) Thermoformed glass fiber reinforced polypropylene: Microstructure, mechanical properties and residual stresses, *Polym Compos* **19**:301–309.

[4] Gupta V B, Mittal R K, Sharma P K, Mennig G and Wolters J (1989) Some studies on glass fiber-reinforced polypropylene. Part II: Mechanical properties and their dependence on fiber length, interfacial adhesion, and fiber dispersion, *Polym Compos* **10**:16–27.

[5] Thorby D (2008) *Structural Dynamics and Vibration in Practice*, Butterworth-Heinemann, Amsterdam, 1st edn.

[6] Peterlin A (1972) Mechanical Properties of Polymeric Solids, *Ann Rev Mater Sci* **2**:349–380.

[7] Takemori M T (1984) Polymer Fatigue, *Ann Rev Mater Sci* **14**:171–204.

[8] Crist B (1995) The Ultimate Strength and Stiffness of Polymers, *Ann Rev Mater Sci* **25**:295–323.

[9] Pegoretti A (2009) Creep and Fatigue Behavior of Polymer Nanocomposites, in *Nano- and Micro-Mechanics of Polymer Blends and Composites* (Eds. Karger-Kocsis J and Fakirov S), Hanser, Munich, chap. 9, pp. 301–339.

[10] Brown H R, Kramer E J and Bubeck R A (1988) Effect of deformation ratio on fibril deformation in fatigue of polystyrene, *J Mater Sci* **23**:248–252.

[11] Toki S, Sics I, Burger C, Fang D, Liu L, Hsiao B S, Datta S and Tsou A H (2006) Structure evolution during cyclic deformation of an elastic propylene-based ethylene-propylene copolymer, *Macromolecules* **39**:3588–3597.

[12] Stribeck N, Nöchel U, Funari S S and Schubert T (2008) Tensile Tests of Polypropylene Monitored by SAXS. Comparing the Stretch-Hold Technique to the Dynamic Technique, *J Polym Sci Polym Phys* **46**:721–726.

[13] Stribeck N (2009) Deformation behavior of nanocomposites studied by X-ray scattering: Instrumentation and methodology, in *Nano- and Micromechanics of Polymer Blends and Composites* (Eds. Karger-Kocsis J and Fakirov S), Hanser Publisher, Munich, vol. 1, chap. 8, pp. 269–300.

[14] Denchev Z, Dencheva N, Funari S S, Motovilin M, Schubert T and Stribeck N (2010) Nanostructure and mechanical properties studied during dynamical straining of microfibrillar reinforced HDPE/PA blends, *J Polym Sci Part B Polym Phys* **48**:237–250.

[15] Stribeck N (2007) *X-Ray Scattering of Soft Matter*, Springer, Heidelberg, New York.

[16] Stribeck N (2001) Extraction of domain structure information from small-angle X-ray patterns of bulk materials, *J Appl Cryst* **34**:496–503.

[17] Ruland W (1977) The evaluation of the small-angle scattering of lamellar two-phase systems by means of interface distribution functions, *Colloid Polym Sci* **255**:417–427.

[18] Vonk C G (1979) A SAXS study of PE fibers, using the two-dimensional correlation function, *ColloidPolym Sci* **257***:1021–1032.*

[19] Debye P and Bueche A M (1949) Scattering by an Inhomogeneous Solid, *J Appl Phys* **20**:518–525.

[20] Porod G (1951) The Small-Angle X-Ray Scattering from densely packed colloidal systems (Ger.), *Colloid Polym Sci* **124**:83–114.

[21] Vonk C G (1973) Investigation of Non-Ideal Two-Phase Polymer Structures by Small-Angle X-ray Scattering, *J Appl Cryst* **6**:81–86.

[22] Baltá Calleja F J and Vonk C G (1989) *X-Ray Scattering of Synthetic Polymers*, Elsevier, Amsterdam.

[23] Zeinolebadi A and Stribeck N (2010) Exploring a pathway for time-resolved studies of polymer fatigue related to nanostructure evolution, *IOP Conf Ser Mater Sci Eng* **14**:012010.